Chapter 3

# Above-Ground Biomass Estimation with High Spatial Resolution Satellite Images

Adélia M. O. Sousa, Ana Cristina Gonçalves and José R. Marques da Silva

Additional information is available at the end of the chapter

http://dx.doi.org/10.5772/65665

**Abstract**

Assessment and monitoring of forest biomass are frequently done with allometric functions per species for inventory plots. The estimation per area unit is carried out with an extrapolation method. In this chapter, a review of the recent methods to estimate forest above-ground biomass (AGB) using remote sensing data is presented. A case study is given with an innovative methodology to estimate above-ground biomass based on crown horizontal projection obtained with high spatial resolution satellite images for two evergreen oak species. The linear functions fitted for pure, mixed and both compositions showed a good performance. Also, the functions with dummy variables to distinguish species and compositions adjusted had the best performance. An error threshold of 5% corresponds to stand areas of 8.7 and 5.5 ha for the functions of all species and compositions without and with dummy variables. This method enables the overall area evaluation, and it is easily implemented in a geographic information system environment.

**Keywords:** QuickBird, multi-resolution segmentation, crown horizontal projection, forest inventory, regressions

## 1. Introduction

### 1.1. Role of forest inventories in biomass estimation

Forest covers a larger area on Earth and provides many products and services. Forest evaluation inventories were initiated when wood shortages arose. It can be said that they are the driving force to acquiring information on forest areas, stand composition and products. In the beginning

(Middle Ages), it was focused on timber volume and forest planning. With time demands for products and services changed, shifting their focus [1].

Forest inventories are based on a sampling design for a given threshold error, with ground plot assessment, providing data sets, which enable the forest evaluation. The need for measuring an increasing number of variables to evaluate products and services expected from forests turns them increasingly expensive and labour intensive. Remote sensing enabling the evaluation of some of those variables (*e.g.* areas, stand composition, crown cover) has been included in forests inventories. Though it cannot replace field work, it can rationalise it, allowing sample efficiency and reducing costs, error and labour intensity [1].

Biomass, both above and below ground, estimation, distribution and dynamics have been acquiring an increasing importance, especially in the last couple of decades. It was powered by the use of wood for bioenergy and by the evaluation of carbon stocks, sequestration and losses. The estimation of biomass can be grouped in two main methods: direct and indirect. The *direct method*, thought the most accurate, requires cutting trees, separating their different components (*e.g.* wood, bark, branches and leaves) and determining their dry weight. It is an expensive and labour demanding method, especially in what roots are concerned, which is feasible for small samples and prohibitive for large ones. The *indirect method* is traditionally based on mathematical relations between biomass (dependent variable) and one or a few easy-to-measure tree variables (independent variables). The biomass estimates attained with the former method are used to fit allometric functions at tree level, whose most frequent explanatory variables are the diameter at breast height and/or total height. Up to 2005 for Europe, North America and Australia, many functions were compiled by several authors [2–6]. More recent ones were found [7–12]. This large number of allometric functions stresses their species-specific and site-specific domain, reason why the selection of the best-suited function is of the utmost importance.

The tree-level biomass functions are frequently used to make estimations at plot scale (usually summing the biomass of all stems). Their estimation for a given area is based on the inventory plots (which depend on the sampling design and intensity for a certain error threshold) and an extrapolation method. In the literature, different extrapolation methods are described [1] with accuracy decreasing with the increase in the forest area, the variability of stand composition and structure, topography, soil and climate [13].

The forest inventories have cycles of 5 or 10 years. In between remote sensing can be used to evaluate the forest dynamics, in general, and biomass in particular. On the other hand, advantages can be gained as it can work at different scales and time frames; all area is under evaluation no requiring extrapolation methods; and maps can be produced in a geographical information system (GIS) environment.

A wide range of studies of biomass estimation derived from remote sensing can be found in the literature. In the next subchapter (2), a brief description of the methods and techniques is given. A case study (subchapter 3) will be used to illustrate the development of a methodology which was aimed to be simple and to be used either by researches or by technicians. The challenge was to produce data from remote sensing images for two evergreen oaks (holm and

http://dx.doi.org/10.5772/65665

cork oak), native of the Mediterranean basin, and develop accurate above-ground biomass (AGB) allometric functions whose explanatory variable is crown horizontal projection, for pure and mixed stands of both species, in the latter analysing also the influence of the predictive ability of independent variables that differentiate species and composition.

The innovation of this study is the estimation of above-ground biomass considering or not stand composition, which is identified by the processing of high spatial resolution of satellite image data. In earlier studies, AGB estimation functions using satellite images did not consider the composition as independent variable. In the studies in which medium and low spatial resolution images are used, the pixel size frequently does not allow the separation of the species. High spatial resolution satellite images data enable the identification and delimitation of crowns of different tree species. Nonetheless, the studies with these satellite images seem to be focused in pure stands. The case study presented demonstrates that stand composition improves the accuracy of AGB estimation functions.

### 1.2. Contribution of remote sensing data to biomass estimation

Remote sensing was under a strong development in the last three decades due to the rapid advancement of remote sensing technology, increasing the availability of satellite imagery with different spectral, spatial, radioactive and temporal resolutions. Their sensor technologies enable a wide range of Earth surface monitoring scales [14] of forest areas distribution, species, and physic and biochemical properties [15]. The data can be derived from two sensors: the passive and the active.

In the ***passive sensor***, the optical spectral reflectance of Earth surface is registered. This multi-spectral information is sensitive to vegetation characteristics such as their shadows and textures, tree density, leaf area index (LAI) and crown size [16]. Good correlations are found between the former and the latter, namely with biomass [17] for a wide range of geographical areas [18]. To develop biomass functions, several methods are used. The most frequent is the regression analysis using forest inventory biomass data and satellite generated data [19], such as spectral reflectance, crown diameter and crown horizontal projection [20–24], original bands and/or vegetation indices [25–28]. The green vegetation canopy has different interactions with specific electromagnetic spectrum ranges, especially the red (R) and the near infrared (NIR) regions, due to the leaves photosynthetic activity and thus with LAI and biomass. The middle infrared (MIR) region, because of its ability to normalise the canopy cover variability, plays also an important contribution [15]. High relations are established between spectral reflectance and/or vegetation indices, and canopy structure, LAI or biomass [16] from tropical [29, 30] to Mediterranean evergreen oaks and shrubland [17, 26, 31, 32] landscapes. Vegetation indices, condensing satellite imagery data in a quantitative numeric form, are related to some forest parameter's estimation, such as the number of trees per hectare [33], canopy cover [26, 34] and volume, basal area and biomass [35]. The aforementioned indices show a better sensitivity when compared with the spectral reflectance [36]. Apart from regression, other methods are described in the literature, such as k-nearest neighbour, neural network, regression tree, random forest and support vector machine [29, 37–40].

Passive sensor, satellite imagery data, depends on its spatial resolution to determine directly the working scale and can be divided into three groups: low, medium and high.

The ***low spatial resolution*** satellite imagery data are characterised by scenes covering large geographical areas. The first studies of biomass estimation at local, regional and global scales used the images from the National Oceanic and Atmosphere Administration (NOAA) with the Advanced Very High Resolution Radiometer (AVHRR) sensor, with 1.1 km of spatial resolution; Moderate Resolution Imaging Spectroradiometer (MODIS), with 500 m [23]; and Satellite *Pour l'Observation de la Terre* (SPOT) Vegetation with 1 km of spatial resolution [41]. The advantage that can be pointed out in the biomass estimation with this spatial resolution is that one scene covers large area allowing working at country and global scales. Conversely, the pixel size makes the image classification more difficult due to the different land cover types encountered in it, resulting frequently in low accuracy biomass estimations [42]. To surpass this disadvantage in some studies, spectral mixture analysis was employed, where each pixel is a physical mixture of the multiple components weighted by the dominant area and the mixture spectrum is a linear combination of the endmember reflectance spectra [43].

The ***medium spatial resolution*** (30 m) satellite imagery data more frequently used result from the processing of Landsat Thematic Mapper (TM), Enhanced Thematic Mapper Plus (ETM +), Advanced Spaceborne Thermal Emission and Reflection radiometer (ASTER) and Wide Field Sensors (WiFS) [23, 25, 44, 45]. The data set is usually combined with forest inventory sample plots data and low spatial resolution imagery. Examples of the first are the volume and biomass estimation of conifer species of boreal forest in northern Europe, with Landsat images and NOAA-AVHRR [46] and Landsat and WiFS [25]; example of the second is AGB estimation for local and regional scales [25, 39, 46].

The data of ***high spatial resolution*** (IKONOS, QuickBird, WordView 2) have had, more recently, a high availability increase. Improved accuracy in biomass estimation is reached when compared with the former two spatial resolutions. The main disadvantage derives from their spatial resolution, which makes the data processing more time-consuming, thus better suited for local or regional scales [27]. In the literature, some references were found for these data sets, but few for biomass estimation, most of which with functions developed with regression analysis methods. Examples with IKONOS image data are the estimation of wet and dry biomass of oil palm plantations in Africa, considering vegetation indices and individual reflectance bands [47] and allometric equations of diameter at breast height and AGB as a function of crown width in tropical forests [48]. Examples with QuickBird are a methodology to estimate and map AGB for black spruce stands in Canada with shadow fraction as explanatory variable [49], AGB functions whose independent variable is crown horizontal projection, applying multi-resolution segmentation and object-oriented classification methods, with regression analysis for *Eucalyptus* sp. and *Tectona grandis* L. [50] and *Quercus rotundifolia* [51].

The three referred spatial resolutions of the optical remote sensing imagery for the same region and their image processing techniques allow the monitoring of AGB with different degrees of detail which are able to decrease the processing time and costs [19, 27, 52].

http://dx.doi.org/10.5772/65665

The ***active sensor*** is based on a mechanism that transmits and receives a portion of energy (microwaves region), interacting with Earth surface, and whose relevance to modelling forest variables depends on how deep the signal penetrates in the canopy. The mostly used data are derived from the Space-borne synthetic Aperture Radar (SAR) and L-band ALOS PALSAR. Two groups of data can be defined: RAdio Detection And Ranging (RADAR) and Light Detection and Ranging (LiDAR). The ***RADAR*** data's main advantage is their independence of atmospheric conditions as wavelength of radiation is much larger that the atmospheric particles [53], reason why it has acquired a marked importance in regions with frequent cloud cover [15]. Several examples of AGB estimation with RADAR were found in the literature [54–59]. The ***LiDAR*** is mainly obtained by airborne discrete-return [60], airborne waveform and from ground-based [61] LiDAR. Several authors developed nonlinear functions for AGB with its derived variables [15, 62] for individual trees, plot and stands, depending on the type of LiDAR system used [16]. LiDAR derives forest structural information (canopy cover), and RADAR backscatter seems to be able to estimate AGB with good accuracy [63].

In summary, the estimation of forest AGB with remote sensing data has advantages and disadvantages. To obtain very good accuracy, these approaches need a heavy field work in order to attain training data sets. However, many studies present methodologies with very good results at local, regional and global scale for AGB estimation. There is a trend towards the combination of several types of remote sensing imagery data to generate vegetation parameters and their relation with forest biomass.

## 2. Case study

### 2.1. Introduction

The data resulting from passive sensors, with low and medium spatial resolution, are usually used for the country or global scales. Due to their pixel size, it is not possible to identify and delimitate the tree crowns. Conversely, high spatial resolution satellite images enable it with good accuracy. The active sensors processing is more difficult than the passive sensors. Thus, when developing a methodology to be used both by researches and by technicians, the passive sensors data processing is more straightforward than that of the active sensors. The objectives of this study are the development of allometric functions for the estimation of AGB with crown horizontal projection, obtained with high spatial resolution satellite image, as independent variable with linear regression for (i) cork oak pure stands, (ii) mixed cork oak and holm oak stands (from this point forward referred as evergreen oaks) and (iii) both pure and mixed stands (from this point forward referred as all). Though with similar stand parameters there are some differences between pure stands of cork oak or holm oak and mixed stands of both species. Thus it was considered that the model for both species might be improved with the inclusion of dummy variables for species and composition as independent variables.

Cork oak (*Quercus suber* L.) and holm oak (*Quercus rotundifolia* Lam.) are native of the Mediterranean basin, distributed from Portugal to Greece and Portugal to Syria [64]. These species occur usually in low-density stands in a silvopastoral system, called *montado*, with open heterogeneous canopies, where the main products are bark and fruit, associated with extensive

grazing, both in pure and in mixed stands. According to the Portuguese National Forest Inventory, cork oak and holm oak stands account for 22.5 and 13.7% of the forest area, respectively. The biomass for pure cork oak stands is 49.5 t/ha with an error of 5.2% and for holm oak 23.2 t/ha with an error of 7.2%. Mixed stands with cork oak or holm oak as dominant species correspond to 17% of their total area. The biomass estimation for mixed stands is 35.6 t/ha with an error of 13.7% [65]. They are similar in terms of habit, especially due to pruning to enhance fruit production and growth; both are slow growing [64].

## 2.2. Materials and methods

### *2.2.1. Study area*

The study area is in southern Portugal, region of Mora, with approximately 80 km$^2$ (**Figure 1**). The area is mainly occupied by forest, composed predominantly by cork and holm oak in both pure and mixed stands. This region has a Mediterranean climate with a hot and dry summer and rainy winter with lower temperature. The terrain is characterised by small variations, with a mean elevation of about 200 m. The used QuickBird satellite image (August 2006) has a spatial resolution of 0.70 m, resulting from a fusion of panchromatic band with the four multi-spectral bands, blue (B), green (G), red (R) and near infrared (NIR).

### *2.2.2. Processing satellite image*

The image was geometric and radiometric corrected using ENVI4.8 [66]. The geometric correction was based on ground control points obtained with Global Navigation Satellite System (GNSS) and geodetic vertices, identified on the ground and in the images, with a Root Mean Square Error (RMSE) of 0.49 m. The pixel values that are the digital numbers of the image were converted to top-of-atmosphere reflectance and finally to soil reflectance, using the dark object subtraction method [67]. The Normalized Difference Vegetation Index (NDVI) [68] was calculated with the latter and used to generate a vegetation mask, isolating tree crowns from other land cover types. For this propose, the multi-resolution segmentation method with the contrast split segmentation algorithm on eCognition, version 8.0.1 was applied [69]. Over this vegetation mask, forest species were identified using the nearest neighbour classification method, producing a map with the delimitation of trees crowns identified by specie [70].

The area was divided into a square grid of 45.5 m× 45.5 m (2070.25 m$^2$). Grids were classified according to the species present. The crown cover obtained with satellite data ($CC_s$) was defined as the percentage of area occupied by the crown horizontal projection per grid ($CHP_s$) in relation to the grid area. It was calculated with the vegetation mask per species using a geographic information system, ArcGIS, version 10 [71]. A grid was considered pure when crown cover of one species was equal or larger than 75% and mixed otherwise. The design of the forest inventory was a random stratified sampling by proportional allocation. Three strata were defined as function of crown cover: (i) 10–30%, (ii) 30–50% and (iii) >50%.

http://dx.doi.org/10.5772/65665


**Figure 1.** Location of the study area (dark grey) and Alentejo region (light grey).

### *2.2.3. Forest inventory data and biomass estimation*

Forest inventory data set is composed of 17 plots of pure holm oak, 11 plots of pure cork oak and 23 mixed plots of holm oak and cork oak, with a total sampled area of 10.6 ha. In these plots, for all individuals with a breast height diameter ≥6 cm, the diameter at breast height, total height and crown radii in four directions (North, South, East and West) were measured [72]. Each tree geographical location was recorded by GNSS. Tree crown horizontal projection ($CHP_p$) was calculated as the circle whose radius is the arithmetic mean of the four crown radii measured. The relation (in %) of sum of the tree crown horizontal projections to plot area was used to estimate plot crown cover ($CC_p$). Ref. [8] developed a biomass allometric function per tree with simultaneous fitting for cork and holm oak. As the stands referred by the aforementioned authors were similar to those of this study, their functions were used to estimate above-ground biomass ($AGB$, Eq. (1)) as the sum of wood ($ww$), bark ($wb$) and crown ($wc$) biomass. Above-ground biomass per plot ($AGB_p$) was defined as the sum of $AGB$ of all the trees in the plot.

$$AGB_t = ww + wb + wc = 0.164185 \times dbh^{2.011002} + 0.600169 \times dbh^{1.355957} + 1.909152 \times dbh^{1.200354} \quad (1)$$

### *2.2.4. Statistical analysis*

Statistical analysis included correlation analysis and linear and multiple regression, implemented in R statistical software [73]. As $AGB_p$, $CHP_p$ and $CHP_s$ did not have normal distribution (evaluated with Shapiro-Wilk normality test), the Spearman correlation test was used. The linear function was selected as it is especially suited for one layer or without crown closure stands or forests [26]. As it was assumed that null *CHP* corresponded to null *AGB*, the linear regression through the origin (Eq. (2), where $\beta$ is the slope) was used. The ordinary least square linear method was selected to fit the functions, both for the individual and for their cumulative values (**Figure 2**.) with $CHP_s$ as independent variable. Also, in order to understand whether AGB could be estimated with aforementioned models, a preliminary analysis was carried out for plot inventory data ($CHP_{pi}$) with the same methodology for cork oak, evergreen oaks and all plots. The preliminary analysis for holm oak was done by [51], and the data were included in the evaluation for all plots in this study.

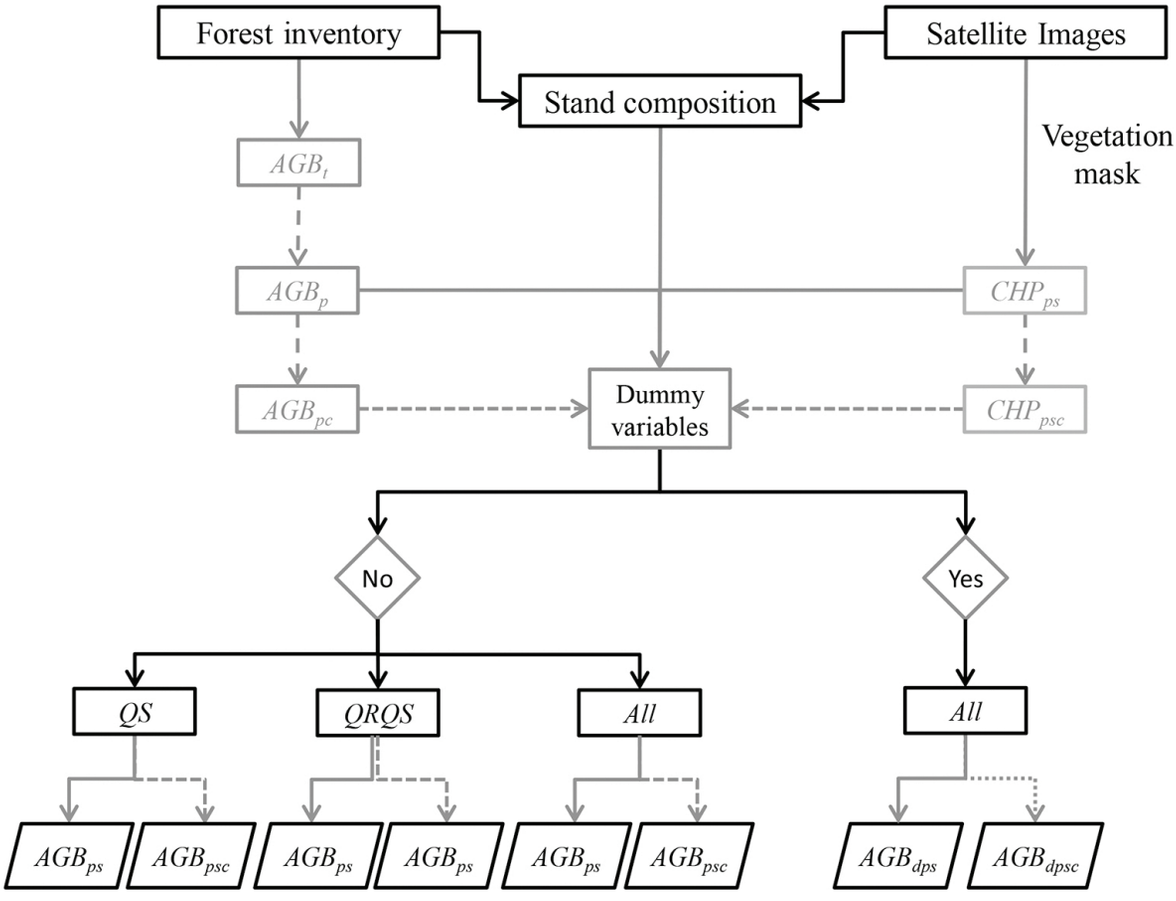


**Figure 2.** Flow diagram of the models developed (where AGB is the above-ground biomass in kg, CHP is the crown horizontal projection in $m^2$, t is the tree, p is the plot values, i is the inventory data, c is the cumulative values, s is satellite image data and d is dummy variables).

As the goal was to develop functions able to estimate AGB as function of *CHP* for the two evergreen oaks, in pure and mixed stands, dummy variables were defined to test the species composition contribution in the function predictive ability (**Figure 2**). Three dummy variables were defined. For each dummy variable, 1 indicates that the plot is pure holm oak (*dQR*), pure cork oak (*dQS*) or mixed holm oak and cork oak (*dQRQS*) and 0 otherwise. Multiple linear regression with stepwise method, using Akaike information criterion (AIC) as selection criteria, was used to fit the allometric functions (Eq. (3), where $\beta_i$ are the regression coefficients, i = 0, 1, 2, 3). Multicollinearity among explanatory variables was analysed with variance inflation factor (VIF), considering that values exceeding 10 are sign of serious multicollinearity [74, 75].

As suggested by several authors [76, 77], the models were studied by the sum of squares of the residuals (SQR), the coefficient of determination ($R^2$) and the adjusted coefficient of determination ($R^2_{aj}$). Validation tests entail an independent data set. To overtake the inexistence of an independent data set, Refs. [78–80] suggest using predicted residual error. The sum of its square values, PRESS (Eq. (4)), and the sum of its absolute values, APRESS (Eq. (5)), were used as the validation test. The closer to the null value of residuals, the better is the model. The per cent value of the estimated and calculated AGB defined the error.

$$AGB = \beta \times CHP \tag{2}$$

$$AGB = \beta_0 \times CHP + \beta_1 \times dQS + \beta_2 \times dQR + \beta_3 \times dQRQS \tag{3}$$

$$PRESS = \sum_{i=1}^{n} \left( y_i - \hat{y}_{i,-i} \right)^2 \tag{4}$$

$$APRESS = \sum_{i=1}^{n} \left| y_i - \hat{y}_{i,-i} \right|^2 \tag{5}$$

## 2.3. Results and discussion

### *2.3.1. Multi-resolution segmentation and object-oriented classification*

**Figure 3** presents the vegetation mask resulting from the multi-resolution segmentation and object-oriented classification process (yellow line), over the QuickBird image with false colour composite for an area of Mora. The vegetation index NDVI enables a spectral signature sufficiently different to obtain a good distinction of the two forest species (cork and holm oak), with an agreement between the classification and ground truth using Kappa statistic [81, 82], of 78% and a global precision of 89%. Thus, the simultaneous analysis of these two evergreen oak species in pure and mixed stands can be useful for the estimation of AGB and also because,

though they are visually similar, the methodology allows a mapping per species (cork and holm oak) with a good classification accuracy.

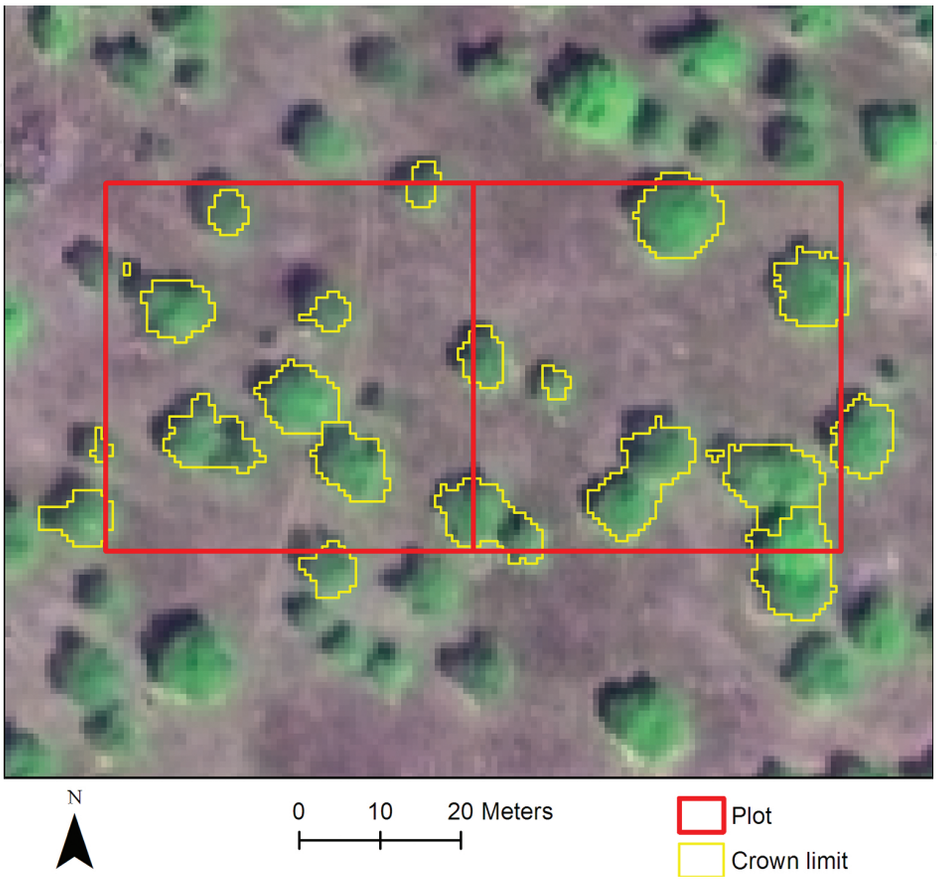


**Figure 3.** QuickBird image with false colour composite (RGB = red, NIR and blue) and illustration of the results of multi-resolution segmentation process (yellow line).

*2.3.2. Individual trees and plot characteristics and above-ground biomass functions with inventory data*

The descriptive statistics: minimum (*min*), maximum (*max*), arithmetic mean (*mean*), standard variation (*SD*) and coefficient of variation (*CV*) for all plots (*All*), evergreen oaks mixed plots (*QRQS*) and cork pure plots (*QS*) of the data are presented in **Table 1**. The density measures, number of trees per hectare (*N*), basal area per hectare (*G*), crown cover ($CC_s$) and above-ground biomass per hectare (*AGB*) were considered for the inventory data, while crown horizontal projection per plot ($CHP_{ps}$) and crown cover ($CC_s$) were considered for satellite data. In **Table 1**, the differences between the three groups of plots can be observed. Comparing the descriptive statistics of cork oak pure plots with those of evergreen oak plots (**Table 1**), higher densities and *AGB* are observed for the former. A more detailed analysis at tree level reveals that in the mixed plots about 54% of the trees are holm oak and 46% are cork oak. The differences are, at least partially, explained by the individual tree dimensions. While in the mixed plots mean crown radius is equal for both species (3.1 m) and similar to the cork oak pure plots (3.0 m), the mean total height and the mean quadratic diameter ($d_g$) are different:

6.8 m, 7.1 m, 35.8 cm and 37.6 cm, respectively. This is also reflected in the $AGB_t$ with a mean larger for the cork oak pure plots (463.9 kgtree$^{-1}$) than for the mixed plots (424.0 kgtree$^{-1}$). When the two species are analysed in the evergreen oak plots, the cork oak individuals have, in average, larger dimensions (7.1 m of total height and 38.4 cm of $d_g$) than the holm oak ones (6.3 and 33.6 cm), which is also reflected in the mean $AGB_t$ (481.7 and 382.3 kgtree$^{-1}$, respectively). The diameter distribution of the evergreen oak plots covers a wide spam indicative of stands of several cohorts (or age classes). The species spatial distribution visual analysis point outs towards an individual distribution both by species and by cohort. This might be probably due to the mutualistic and competitive interactions [83] and also by the sociability and compatibility [84] of these oaks, with similar growth rates, both slow, and rotation length. The holm oak pure plots [51] have values between the former two compositions. Also, trees with similar crown sizes may have quite different $AGB_t$. This is expectable considering two factors. First, these species have weak epinastic control, but when in group tend to reduce their lateral development due to branch abrasion or to the effects of high and low shading [83], especially because they are shade intolerant. As in *montado* tree spatial distribution is sparse, though irregular, trees can be found isolated or in clusters and in the latter is the competition phenomenon that explains, at least partially, the variability in crown dimensions. Second, in the *montado* system pruning to enhance fruit production is frequent [64] in mature stands and this reverses temporarily the rate between $CHP_t$ and $AGB_t$.

| | **All plots (*All*)** | | | | | **Evergreen oaks mixed plots (*QRQS*)** | | | | | **Cork oak pure plots (*QS*)** | | | | |
|---|---|---|---|---|---|---|---|---|---|---|---|---|---|---|---|
| **Variables** | **min** | **max** | **mean** | **SD** | **CV** | **min** | **max** | **mean** | **SD** | **CV** | **min** | **max** | **mean** | **SD** | **CV** |
| *N* (treesha$^{-1}$) | 19 | 140 | 70 | 28 | 40.5 | 19 | 140 | 61 | 28 | 46.5 | 53 | 135 | 88 | 24 | 27.7 |
| *G* (m$^2$ha$^{-1}$) | 2.6 | 15.4 | 7.1 | 2.7 | 38.1 | 2.6 | 13.1 | 6.2 | 2.1 | 34.3 | 5.2 | 15.4 | 9.8 | 3.0 | 31.2 |
| *CCp* (%) | 8.7 | 49.3 | 25.3 | 9.2 | 36.5 | 8.7 | 49.3 | 20.9 | 8.2 | 39.3 | 18.7 | 42.3 | 27.5 | 7.4 | 26.8 |
| *CCs* (%) | 13.7 | 70.5 | 35.0 | 14.7 | 41.9 | 14.3 | 58.8 | 28.5 | 11.2 | 39.2 | 23.6 | 70.5 | 44.9 | 13.5 | 30.0 |
| $CHP_{ps}$ (m$^2$) | 284.2 | 1460.2 | 725.3 | 303.7 | 41.9 | 296.9 | 1216.7 | 589.3 | 230.9 | 39.2 | 489.0 | 1460.2 | 928.7 | 278.7 | 30.0 |
| *AGB* (tha$^{-1}$) | 10.4 | 62.7 | 30.1 | 11.1 | 36.8 | 10.4 | 51.5 | 26.0 | 8.6 | 33.1 | 23.8 | 62.7 | 40.7 | 11.9 | 29.2 |

N: number of trees per hectare, G: basal area per hectare, $CC_s$: crown cover calculated with satellite data, $CHP_{ps}$: plot crown horizontal projection evaluated with satellite data, AGB: above-ground biomass per hectare, min: minimum, max: maximum, mean: arithmetic mean, SD: standard variation, CV: coefficient of variation.

**Table 1.** Descriptive statistics.

The strongest positive correlations are found for pure plots of cork oak between $AGB_p$ and $CHP_p$ (0.827), expected due to the smaller variability (**Table 1**). Strong positive correction for pure cork oak plots between $AGB_p$ and $CHP_s$ was attained (0.627). The difference between $AGB_p$ and $CHP_s$ and $CHP_p$ can be, at least partially, explained by the stems spatial distribution, the shade casted by trees and understory. In tree clusters, multi-resolution segmentation process is not able to isolate tree crowns, including mixed pixels of vegetation, soil and/or shadow inside the polygon that delimitates the cluster. Some types of understory vegetation, near tree crowns, have similar spectral signature, and when delimiting the crown those pixels are

included [85, 86]. The weakest correlations were observed for the evergreen oak plots between $AGB_p$ and $CHP_p$ (0.482) and $CHP_s$ (0.552), which is expected due to the variability increase in those parameters. When all the plots are considered, strong positive correlations are found between $AGB_p$ and $CHP_p$ (0.671) and $CHP_s$ (0.746).

| Model | Plots | Equation | SQR | $R^2$ | $R^2_{aj}$ | PRESS | APRESS |
|---|---|---|---|---|---|---|---|
| | | **Inventory data** | | | | | |
| 1 | QS | $AGB_{pi\_QS} = 14.7087 \times CHP_{pi\_QS}$ | 23576825 | 0.972 | 0.969 | 0.00000019 | 0.00101252 |
| 2 | QRQS | $AGB_{pi\_QRQS} = 11.5889 \times CHP_{pi\_QRQS}$ | 74401387 | 0.899 | 0.894 | 0.00000065 | 0.00313966 |
| 3 | All | $AGB_{pi\_All} = 11.4139 \times CHP_{pi\_All}$ | 187602462 | 0.916 | 0.915 | 0.00000113 | 0.00631091 |
| 4 | QS | $AGB_{pic\_QS} = 14.8889 \times CHP_{pic\_QS}$ | 16220130 | 0.9995 | 0.999 | 0.00000002 | 0.00034940 |
| 5 | QRQS | $AGB_{pic\_QRQS} = 11.75374 \times CHP_{pic\_QRQS}$ | 292087434 | 0.997 | 0.997 | 0.00000004 | 0.00049897 |
| 6 | All | $AGB_{pic\_All} = 11.75374 \times CHP_{pic\_All}$ | 3066829502 | 0.998 | 0.998 | 0.00000001 | 0.00049770 |
| | | **Satellite image data** | | | | | |
| 7 | QS | $AGB_{ps\_QS} = 8.847 \times CHP_{ps\_QS}$ | 40091932 | 0.953 | 0.948 | 0.00000016 | 0.00106716 |
| 8 | QRQS | $AGB_{ps\_QRQS} = 8.5093 \times CHP_{ps\_QRQS}$ | 72931734 | 0.901 | 0.896 | 0.00000061 | 0.00317184 |
| 9 | All | $AGB_{ps\_All} = 8.1309 \times CHP_{ps\_All}$ | 163946315 | 0.927 | 0.925 | 0.00000120 | 0.00656152 |
| 10 | QS | $AGB_{psc\_QS} = 9.2671 \times CHP_{psc\_QS}$ | 43379144 | 0.999 | 0.998 | 0.00000001 | 0.00025905 |
| 11 | QRQS | $AGB_{psc\_QRQS} = 9.037 \times CHP_{psc\_QRQS}$ | 104841889 | 0.999 | 0.999 | 0.00000005 | 0.00068011 |
| 12 | All | $AGB_{psc\_All} = 8.85869 \times CHP_{psc\_All}$ | 1722352935 | 0.999 | 0.999 | 0.00000001 | 0.00050963 |
| | | **Satellite image data with dummy variables** | | | | | |
| 13 | All | $AGB_{dps} = 4.836 \times CHP_{ps} + 2191.3997 \times dQR + 3944.2222 \times dQS + 2532.8074 \times dQSQR$ | 104975100 | 0.953 | 0.949 | 0.00000151 | 0.00661458 |
| 14 | All | $AGB_{dpsc} = 8.6029 \times CHP_{psc} + 6425.9261 \times dQR + 6105.1531 \times dQS + 4827.1112 \times dQSQR$ | 1235713930 | 0.991 | 0.999 | 0.00000007 | 0.00070861 |

AGB: above-ground biomass in kg, CHP: crown horizontal projection in $m^2$, p: plot, i: inventory data, c: cumulative values, s: satellite data, QS: cork oak, QSQR: evergreen oaks, All: all plots, d: dummy variable.

**Table 2.** Properties of the fitted models.

The statistical properties and the PRESS and APRESS statistics of the linear models for plot $CHP_{pi}$ (models 1–3) and $CHP_{pic}$ (models 4–6) are indicative of their good performance (**Table 2**).

http://dx.doi.org/10.5772/65665

When comparing the models for the four sets of plots, the statistical properties of the pure plots are better than those of the evergreen oak plots and all plots (**Table 2**), due to the increase in variability in the latter two. The results attained by [51] for holm oak pure plots are also better when compared with the evergreen oak and all plots of this study. Nonetheless, smaller differences in model performance are found for models 4–6 when compared with models 1–3. The differences might be partially due to the small differences in habit of the two species, the spatial distribution pattern of the individuals of both species and silvicultural practices, especially pruning where focus is put in the crown enlargement more for holm oak than for cork oak. This is also reflected in the overall model error. Larger overall errors are found for the models 2 and 3 (24.3% and 23.7%, respectively) when compared with model 1 (13.6%), and models 5 and 6 (9.8% and 9.2%, respectively) when compared with model 4 (4.4%).

*2.3.3. Above-ground biomass allometric functions with satellite image data*

The statistical properties and the validation statistics of the linear models for $CHP_{ps}$ and $CHP_{psc}$ for pure cork oak plots (models 7 and 10), for evergreen oak plots (models 8 and 11) and for all plots (models 9 and 12, **Figure 4a**, **b**) are indicative of their good performance (**Table 2**). These results are in accordance with [26] that states that linear regression behaves well in stands with one layer, while [47] refers that in multi-layered stands nonlinear functions are better suited. Noteworthy is that models 10–12 have better statistical properties than the models 7–9. When comparing the models for evergreen oaks with those for pure plots, the statistical properties of the former are worse than of latter (**Table 2**). This, as already referred, is due to the larger variability observed in the mixed plots. When comparing the models fitted with inventory and satellite image data, the performance is better for the former, which can be partially explained by the differences in the calculation of *CHP* with the sets of data. Models for cumulative values have slightly better performance for the inventory (models 4–6) than for the satellite image data (models 10–12), corroborated by the overall error of 3.7, 4.4, 9.8 and 9.2%, and 13.4, 4.8, 6.4 and 5.8%, respectively.

Model 10, for cork oak pure stands, has larger errors up to 4000 $m^2$ and an irregular trend afterwards. For error thresholds of 10 and 5% *CHP,* areas larger than 4000 and 5000 $m^2$, respectively, are needed. Considering a mean *CHP* area of 4486 $m^2ha^{-1}$, the corresponding stand area is 0.9 and 1.1 ha, respectively. Model 11, for evergreen oak stands, shows higher errors than the former models for *CHP* areas up to 1000 $m^2$, with a continuous decrease, in absolute value, up to 3000 $m^2$ and stabilisation afterwards. Errors smaller or equal than 10 and 5% are attained for *CHP* areas of 3000 and 7000 $m^2$, respectively. The mean *CHP* area for these stands is 2847 $m^2ha^{-1}$, which corresponds to the above-referred errors to stand areas of 1.1 and 2.5 ha, respectively. Model 12, for both pure and mixed stands, shows the same error trend as model 11. Errors below the aforementioned are attained for *CHP* areas of 2000 and 8000 $m^2$. As the mean *CHP* area is 3503 $m^2ha^{-1}$, the corresponding stand areas are 0.6 and 2.3 ha. As 92% of the holm oak stands and 89% of the cork oak stands have areas bigger than 2 ha [65], this allometric function can be used at local and regional level.

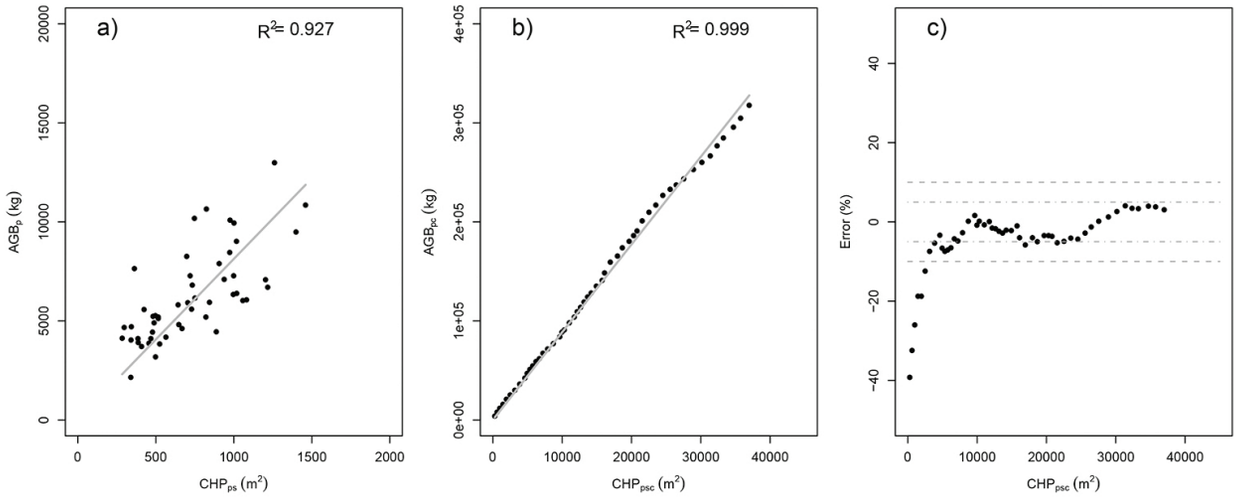


**Figure 4.** Crown horizontal projection derived from satellite image per plot ($CHP_{ps}$) versus above-ground biomass per plot ($AGB_p$) and equation (in grey) for model 9 (a) and their cumulative values, $CHP_{psc}$ vs $AGB_{pc}$, and equation (in grey) (b) and error (c) for model 12.

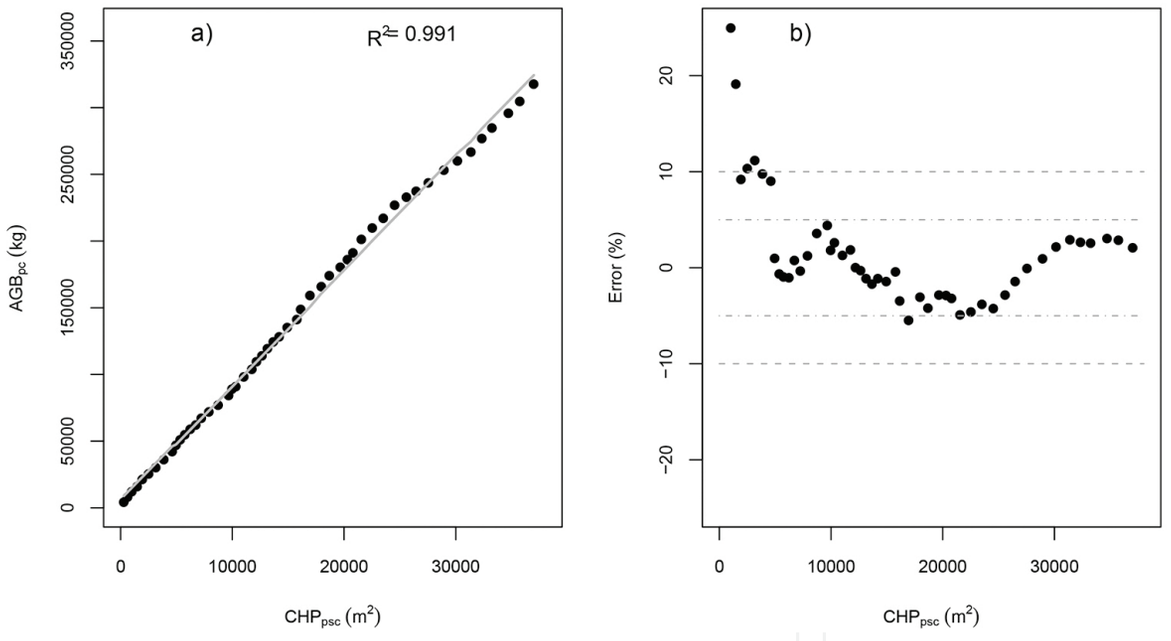


**Figure 5.** Cumulative values of crown horizontal projection derived from satellite image per plot ($CHP_{psc}$) versus cumulative values of above-ground biomass per plot ($AGB_p$) and equation (in grey, a), and error distribution (b) for model 14.

The inclusion of independent variables identifying the plot composition originated a generalised improvement in the statistical properties of the models (**Table 2**) for $CHP_{ps}$ (model 13) and $CHP_{psc}$ (model 14), when compared with those without composition variables (models 9 and 12). In fact, plot composition has revealed important as for both models the three dummy variables were included. Also, multicollinearity did not present any problem as VIF values

were always lower than 10, being for *CHP*, *dQR*, *dQS* and *dQRQS*, 8.5, 3.8, 3.6 and 3.2 for model 13, and 4.6, 1. 8, 3.0 and 1.8 for model 14, respectively. The models accuracy increases from the models with only *CHP* (9 and 12) to those that include the dummy variables (models 13 and 14). Noteworthy is also the decrease in SQR of 36% from models 9 to 13, and of 39% from models 12 to 14, with the corresponding increase in the adjusted regression coefficients. There is a considerable improvement in the overall error from models 9 to 13, from 23.1 to 5.2% and from models 12 to 14, from 5.8 to 0.1%. The error for model 14 shows an irregular trend with error smaller than 10 and 5% for cumulative crown projection for areas larger than 1500 and 2000 $m^2$, corresponding to stand areas of 0.4 ha and 0.6 ha, respectively (**Figure 5**). Considering the threshold of 5% for model 14, -1.7 ha is needed than for model 12.

All the fitted models (models 7–14) have a high goodness of fit, with more than 90% of the variability explained. It seems that crown horizontal projection as better predictive abilities with linear functions than the shadow fraction processed from QuickBird images [49]. The models developed in this study show also better performances than multiple regression functions with crown diameter and total height as independent variables, derived from a panchromatic band of QuickBird satellite [50] or than exponential functions with reflectance of band 3 or NDVI for IKONOS image [47]. Likewise, biomass estimation functions derived from medium spatial resolution satellite image data do not show as good performance as those obtained in this study. This is probably related to dissimilarity between ground and satellite data [27]. The former was confirmed in a study with Landsat 5 TM and MODIS images for P*inus pinaster* stands, whose independent variable is vegetation indices [17].

### 2.4. Conclusions

Remote sensing gives a good contribution to estimate the above-ground biomass. The high spatial resolution satellite image allows mapping with high accuracy the above-ground biomass at local and regional scale.

The overestimation of crown horizontal projection per plot using high spatial resolution satellite image, when compared with that calculated using inventory data, is related to the inclusion of mixed pixels in the boundary of tree crown delimitation in the multi-resolution segmentation and trees' spatial distribution. Though the cork and holm oak are visually similar, their spectral signature is sufficiently different to obtain a very good classification by forest specie.

In general, above-ground biomass allometric functions for plot and their cumulative values showed a good performance, though better for pure stands than for mixed stands, which might be explained by the larger variability observed in the latter. However, the inclusion of dummy variables, which reflect the differences between the species and the stand structure, originates a generalised improvement in the functions performance. The same threshold errors of 10 and 5% are attained by the latter with less 33 and 70% of the stand areas. Considering that to a 10% error correspond stand areas of 1.1 ha, it includes about 90% of the area occupied by these species in Portugal [65]. This method has the advantage of enabling the overall area evaluation, not requiring forest inventory or extrapolation procedures. It can be used when species composition is not (models 9 and 12) and is (models 13 and 14) differentiated.

## Acknowledgements

The authors would like to thank the forest producers for allowing plot installation and to Paulo Mesquita for satellite image processing. The work was financed by Programa Operativo de Cooperação Transfronteiriço Espanha—Portugal (POCTEP); project Altercexa—Medidas de Adaptación y Mitigación del Cambio Climático a Través del Impulso de las Energías Alternativas en Centro, Alentejo y Extremadura ($Ref_a$ 0317_Altercexa_I_4_E and 0406_ALTERCEXA_II_4_E); TrustEE—innovative market based Trust for Energy Efficiency investments in industry (Project ID: H2020—696140); and National Funds through FCT—Foundation for Science and Technology under the Project UID/AGR/00115/2013.

### Abbreviations

| | |
|---|---|
| AGB | Above-Ground Biomass per tree (kg) |
| $AGB_t$ | tree Above-Ground Biomass per tree (kg) |
| AIC | Akaike Information Criterion |
| *All* | all plots |
| ALOS | Advanced Land Observing Satellite |
| APRESS | Absolute Predicted Residual Error Sum |
| ASTER | Advanced Spaceborne Thermal Emission and Reflection Radiometer |
| AVHRR | Advanced Very High Resolution Radiometer |
| *c* | cumulative values |
| *CC* | Crown Cover (%) |
| *CHP* | Crown Horizontal Projection ($m^2$) |
| CV | Coefficient of Variation |
| d | dummy variable |
| *dbh* | diameter at breast height, measured at 1.30 m height (cm) |
| dg | mean quadratic diameter (cm) |
| G | basal area per hectare ($m^2ha^{-1}$) |
| GNSS | Global Navigation Satellite System |
| *i* | inventory data |
| ETM + | Enhanced Thematic Mapper + |
| LAI | Leaf Area Index |
| max | maximum value |
| mean | arithmetic mean value |
| min | minimum value |
| MODIS | Moderate Resolution Imaging Spectroradiometer |
| N | number of trees per hectare (tree $ha^{-1}$) |
| NDVI | Normalized Difference Vegetation Index |

| | |
|---|---|
| NOAA | National Oceanic and Atmospheric Administration |
| *p* | plot |
| PALSAR | Phased Array type L-band Synthetic Aperture Radar |
| PRESS | Predicted Residual Error Sum of Squares |
| QR | holm oak (*Quercus rotundifolia*) pure plots |
| QRQS | mixed plots of holm and cork oaks (evergreen oaks) |
| QS | cork oak (*Quercus suber*) pure plots |
| $R^2$ | coefficient of determination |
| $R^2_{aj}$ | adjusted coefficient of determination |
| RADAR | RAdio Detection And Ranging |
| RMSE | Root Mean Square Error |
| *s* | satellite data images |
| SAR | Space-borne synthetic Aperture Radar |
| SD | Standard Deviation |
| SQR | Sum of Squares of the Residuals |
| *t* | tree |
| TM | Thematic Mapper |
| VIF | Variance Inflation Factor |
| WiFS | Wide Field Sensor |
| *ww* | wood biomass (kg) |
| *wb* | bark biomass (kg) |
| *wc* | crown biomass (kg) |

## Author details

Adélia M. O. Sousa*, Ana Cristina Gonçalves and José R. Marques da Silva

*Address all correspondence to: asousa@uevora.pt

Department of Rural Engineering, School of Sciences and Technology, Institute of Mediterranean Agricultural and Environmental Sciences (ICAAM), Institute of Research and Advanced Information (IIFA), University of Évora, Évora, Portugal

## References

[1] McRoberts R, Tomppo E, Naesset E. Advanced and emerging issues on national forest inventories. Scandinavian Journal of Forest Research. 2010;25:368–381.

[2] Ter-Mikaelian MT, Korzukhin MD. Biomass equations for sixty-five North American tree species. Forest Ecology and Management. 1997;97:1–24.

[3] Eamus D, McGuinness K, William B. editors. Review of Allometric Relationships for Estimating Woody Biomass for Queensland, the Northern Territory and Western Australia, Technical report no. 5a. Australia: Australian Greenhouse Office. 2000. 56p.

[4] Keith H, Barrett D, Keenan R. editors. Review of Allometric Relationships for estimating Woody Biomass for New South Wales, the Australian Capital Territory, Victoria, Tasmania and South Australia, Technical report no. 5b. Australia: Australian Greenhouse Office. 2000. 112p.

[5] Jenkins JC, Chojnacky DC, Heath LS, Birdsey RA. National-scale biomass estimators for United States tree species. Forest Science. 2003;49(1):12–35.

[6] Zianis D, Muukkonen P, Mäkipää R, Mencuccini M. Biomass and Stem Volume equations for tree species in Europe. The Finnish Society of Forest Science, The Finnish Forest Research Institute. Tampere, Finland; 2005. 63p.

[7] Fehrmann L, Kleinn C. General considerations about the use of allometric equations for biomass estimation on the example of Norway spruce in central Europe. Forest Ecology and Management. 2006;236:412–421.

[8] Paulo JA, Tomé M. Equações para estimação do volume e biomassa de duas espécies de carvalhos: *Quercus suber* e *Quercus ilex*. [Equations for estimation of the volume and the biomass of two oak species: *Quercus suber* and *Quercus ilex*]. Publicações do GIMREF; RC1. Instituto Superior de Agronomia, Departamento de Engenharia Florestal. Lisboa. 2006.

[9] Miksys V, Varnagiryte-Kabasinskiene I, Stupak I, Armolaitis K, Kukkola M, Wójcik J. Above-ground biomass functions for Scots pine in Lithuania. Biomass and Bioenergy. 2007;31:685–692.

[10] Correia AC, Faias S, Tomé M, Evangelista M, Freire J, Ochoa P. Ajustamento simultâneo de equações de biomassa de pinheiro manso no Sul de Portugal. [Simultaneous fitting of biomass equations for stone pine in southern Portugal]. Silva Lusitana. 2008;16:197–205.

[11] Djomo AN, Ibrahima A, Saborowski J, Gravenhorst G. Allometric equations for biomass estimations in Cameroon and pan moist tropical equations including biomass data from Africa. Forest Ecology and Management. 2010;260: 1873–1885.

[12] Arias D, Calvo-Alvarado J, Richter DB, Dohrenbusch A. Productivity, aboveground biomass, nutrient uptake and carbon content in fast-growing tree plantations of native and introduced species in the Southern Region of Costa Rica. Biomass and Bioenergy. 2011;35:1779–1788.

[13] Somogyi Z, Cienciala E, Mäkipää R, Muukkonrn P, Lehtonen A, Weiss P. Indirect methods of large-scale forest biomass estimation. European Journal of Forest Research. 2007;126:197–207.

[14] Gail WB. Remote sensing in the coming decade: the vision and the reality. Journal of Application of Remote Sensing. 2007;1(1):012505.

[15] Boyd, DS, Danson FM. Satellite remote sensing of forest resources: three decades of research development. Progress in Physical Geography. 2005;29(1):1–26.

[16] Zhang X, Ni-meister W. Remote sensing of forest biomass. In: Hanes J.M. editor. Biophysical Applications of Satellite Remote Sensing. Springer-Verlag: Berlin Heidelberg; 2014. p. 63–98.

[17] Viana H, Aranha J, Lopes D, Cohen WB. Estimation of crown biomass of *Pinus pinaster* stands and shrubland above-ground biomass using forest inventory data, remotely sensed imagery and spatial prediction models. Ecological Modelling. 2012;226:22–35.

[18] Ahmed T, Tian L, Zhang Y, Ting KC. A review of remote sensing methods for biomass feedstock production. Biomass and Bioenergy. 2011;35:2455–2469.

[19] Pizaña JMG, Hernández JMN, Romero NC. Remote sensing-based biomass estimation. In: Marghny M. editor. Earth and Planetary Sciences, Geology and Geophysics, Environmental Applications of Remote Sensing. Croatia: Intech; 2016. p. 3–40.

[20] Woodcock CE, Collins JB, Jakabhazy VD, Li X, Macomber S, Wu Y. Inversion of the Li-Strahler canopy reflectance model for mapping forest structure. IEEE Transactions on Geoscience and Remote Sensing. 1997;35:405–414.

[21] Phua M, Saito H. Estimation of biomass of a mountainous tropical forest using Landsat TM data. Canadian Journal of Remote Sensing. 2003;29:429–440.

[22] Popescu SC, Wynne RH, Nelson, RF. Measuring individual tree crown diameter with LiDAR assessing its influence on estimating forest volume and biomass. Canadian Journal of Remote Sensing. 2003;29:564–577.

[23] Baccini A, Friedl MA, Woodcock CE, Warbington R. Forest biomass estimation over regional scales using multisource data. Geophysical Research Letters. 2004;31:L10501.

[24] Powell, SL, Warren B, Cohen WB, Healey SP, Kennedy RE, Moisen GG, Pierce KB, Ohmann JL. Quantification of live aboveground forest dynamics with Landsat time-series and field inventory data: a comparison of empirical modelling approaches. Remote Sensing of Environmental. 2010;114:1053–1068.

[25] Tomppo E, Nilsson M, Rosengren M, Aalto P, Kennedy P. Simultaneous use of Landsat-TM and IRS-1C WiFS data in estimating large area tree stem volume and aboveground biomass. Remote Sensing of Environment. 2002;82:156–171.

[26] Carreiras JM, Pereira JMC, Pereira JS. Estimation of tree canopy cover in evergreen oak woodlands using remote sensing. Forest Ecology and Management. 2006;223:45–53.

[27] Lu D. The potential and challenge of remote sensing-based biomass estimation. International Journal of Remote Sensing. 2006;27:1297–1328.

[28] Muukkonen P, Heiskanen J. Biomass estimation over a large area based on standwise forest inventory data and ASTER and MODIS satellite data: a possibility to verify carbon inventories. Remote Sensing of Environment. 2007;107:617–624.

[29] Steininger MK, Steininger, M.K., 2000. Satellite estimation of tropical secondary forest above ground biomass data from Brazil and Bolivia. International Journal of Remote Sensing. 2000;21:1139–1157.

[30] Foody GM, Boyd DS, Cutler MEJ. Predictive relations of tropical forest biomass from Landsat TM data and their transferability between regions. Remote Sensing of Environment. 2003;85:463–474.

[31] Pereira JMC, Oliveira TM, Paul JCP. Satellite-based estimation of Mediterranean shrubland structural parameters. EARSel Advances in Remote Sensing. 1995;4(3–XII): 14–20.

[32] Calvão T, Palmeirim JM. Mapping Mediterranean scrub with satellite imagery: biomass estimation and spectral behaviour. International Journal of Remote Sensing. 2004;25(16):3113–3126.

[33] Joffre R, Lacaze B. Estimating tree density in oak savanna-like 'dehesa' of southern Spain from SPOT data. International Journal of Remote Sensing. 1993;14:685–697.

[34] Salvador R, Pons X. On the applicability of Landsat TM images to Mediterranean forest inventories. Forest Ecology and Management. 1998;104:193–208.

[35] Maciel MNM, Bastos PCO, Carvalho JOP, Watrin OS. Uso de imagens orbitais na estimativa de parâmetros estruturais de uma floresta primária no município de Paragominas, Estado do Pará. [Use of orbital images in the estimation of structural parameters of a primary forest in the municipality of Paragominas, Pará state]. Revista Ciência Agrária. 2009;52:159–178.

[36] Asrar G, Fuchs M, Kanemasu ET, Hatfield JL. Estimating absorbed photosynthetic radiation and leaf area index from spectral reflectance in wheat. Agronomy Journal. 1984;76:300–306.

[37] Nelson RF, Kimes DS, Salas WA, Routhier M. Secondary forest age and tropical forest biomass estimation using Thematic Mapper imagery. BioScience. 2000;50:419–431.

[38] Foody GM, Cutler ME, McMorrow J, Pelz D, Tangki H, Boyd DS, Douglas I. Mapping the biomass of Bornean tropical rain forest from remotely sensed data. Global Ecology & Biogeography. 2001;10:379–387.

[39] Zheng D, Rademacher J, Chen J, Crow T, Bresee M, Le Moine J, Ryu S. Estimating aboveground biomass using Landsat 7 ETM+ data across a managed landscape in northern Wisconsin, USA. Remote Sensing of Environment 2004; 93:402–411

[40] Lu D, Chen Q, Wang G, Liu L, Li G, Moran EA. A survey of remote sensing-based aboveground biomass estimation methods in forest ecosystems. International Journal of Digital Earth. 2016;9(1):63–105.

[41] Fraser RH, Li Z. Estimating fire-related parameters in boreal forest using SPOT VEGETATION. Remote Sensing of Environment. 2002;82:95–110.

[42] Fernández-Manso O, Fernández-Manso A, Quintano C. Estimation pf aboveground biomass in Mediterranean forests by statistical modelling of ASTER fraction images. International Journal of Applied Earth Observation and Geoinformation. 2014;31:45–56.

[43] Tompkins S, John FM, Carld MP, Donald WF. Optimization of Endmembers Mixture Analysis for Spectral. Remote Sensing of Environment. 1997; 59:472–489.

[44] Baccini A, Laporte N, Goetz MS, Dong H. A first map of tropical Africa's above-ground biomass derived from satellite imagery. Environmental Research Letters. 2008;3:045011.

[45] Zhang X, Kondragunta S. Estimating forest biomass in the USA using generalized allometric models and Modis land products. Geophysical Research Letters. 2006;33:L09402.

[46] Häme T, Salli A, Andersson K, Lohi A. A new methodology for the estimation of biomass of conifer-dominated boreal forest using NOAA AVHRR data. International Journal of Remote Sensing. 1997;18(15):3211–3243.

[47] Thenkabail PS, Stucky N, Griscom BW, Ashton MS, Diels J, Meer B, Enclona E. Biomass estimations and carbon stock calculations in the oil palm plantations of African derived savannas using IKONOS data. International Journal of Remote Sensing. 2004;25(23): 5447–5472.

[48] Palace M, Keller M, Asner GP, Hagen S, Braswell B. Amazon forest structure from IKONOS satellite data and the automated characterization of forest canopy properties. Biotropica. 2008;40:141–150.

[49] Leboeuf A, Beaudoin A, Fournier RA, Guindon L, Luther JE, Lambert MC. A shadow fraction method for mapping biomass of northern boreal black spruce forests using QuickBird imagery. Remote Sensing of Environment. 2007;110:488–500.

[50] Upgupta S, Singh S, Tiwari PS. Estimation of aboveground phytomass of plantations using digital photogrammetry and high resolution remote sensing data. Journal of the Indian Society of Remote Sensing. 2015;43(2):311–323.

[51] Sousa AMO, Gonçalves AC, Mesquita P, Marques da Silva JR. Biomass estimation with high resolution satellite images: a case study of *Quercus rotundifolia*. ISPRS Journal of Photogrametric and Remote Sensing. 2015;101:69–79.

[52] Zhu X, Liu D. Improving forest aboveground biomass estimation using seasonal Landsat NDVI time-series. ISPRS Journal of Photogrammetry and Remote Sensing. 2015;102:222–231.

[53] Quegan, S. Recent advances in understanding SAR imagery. In: Danson FM, Plummer SE, editors. Advances in Environmental Remote Sensing. Chichester: Wiley; 1995. p. 89–104.

[54] Imhoff ML. A theoretical analysis of the effect of forest structure on synthetic aperture radar backscatter and the remote sensing of biomass. IEEE Transactions on Geoscience and Remote Sensing. 1995;33:341–52.

[55] Kuplich TM, Freitas CC, Soares JV. 2000. The study of ERS-1SAR and Landsat TMsynergism for landuse classification. International of Remote Sensing. 2000;21(10):2101–2111.

[56] Castel T, Guerra F, Caraglio Y, Hollier F. Retrieval biomass of a large Venezuelan pine plantation using JERS-1 SAR data. Analysis of forest structure impact on radar signature. Remote Sensing of Environment. 2002;79:30–41.

[57] Sun W, Heidt V, Gong P, Xu G. Information fusion for rural land-use classification with high resolution satellite imagery. IEEE Transactions on Geoscience and Remote Sensing. 2003;3(1):3–5.

[58] Santos JR. Airborne Pband SAR applied to the aboveground biomass studies in the Brazilian tropical rainforest. Remote Sensing of Environment. 2003;87:482–493.

[59] Treuhaft RN, Law BE, Asner GP. Forest attributes from Radar interferometric structure and its fusion with optical remote sensing. BioScience. 2004;54:561–71.

[60] Garcia M, Riaño D, Chuvieco E, Danson FM. Estimating biomass carbon stocks for Mediterranean forest in Spain using height and intensity LiDAR data. Remote Sensing of Environment. 2010;114:816–830.

[61] Ni-Meister W, Lee S, Strahler AH, Woodcock CE, Schaaf C, Yao T, Ranson KJ, Sun G, Blair JB. Assessing general relationships between aboveground biomass and vegetation structure parameters for improved carbon estimate from LiDAR remote sensing. Journal of Geophysical Research. 2010;115:1–12.

[62] He Q, Erxue C, An R, Li Y. Above-ground biomass and biomass components estimation using LiDAR data in a coniferous forest. Forests. 2013;4:984–1002.

[63] Tian S, Tanase MA, Panciera R, Hacker J, Lowell K. Forest biomass estimation using radar and LiDAR synergies. In: Proceedings of the IEEE International Geoscience and Remote Sensing Symposium – IGARSS. 21–26 July 2013; Melbourne, Australia: IEEE; 2013. p. 2145–2148.

[64] Correia AV, Oliveira AC. Principais espécies florestais com interesse para Portugal: zonas de influência mediterrânica. [Main forest species with interest for Portugal: zones of Mediterranean influence]. Direcção-Geral das Florestas. Estudos e Informação; 1999. 318p.

[65] IFN5, 2010. Inventário Florestal Nacional. IFN5 2005–2006. Portugal Continental. [National Forest Inventory. IFN5 2005–2006. Continental Portugal]. Autoridade Florestal Nacional, Lisboa.

[66] Envi. Reference Guide—Exelis Visual Information Solutions. Boulder, Colorado: Exelis Visual Information Solutions [Internet]. 2009. Available from: http://www.exelis-vis.com/portals/0/pdfs/envi/envi_zoom_user_guide.pdf. Accessed 2012-11-27.

[67] Chavez Jr. PS. An improved dark-object subtraction technique for atmospheric scattering correction of multispectral data. Remote Sensing of Environment. 1988;24(3): 459–479.

[68] Rouse JW, Haas RH, Schell JA, Deering DW. 1973. Monitoring vegetation systems in the Great Plains with ERTS. In 3rd ERTS Symposium, NASA SP-351 I. 309–317.

[69] Definiens Imaging. eCognition Developer 8.0.1 Reference Book [Internet]. 2010. Available from: http://www.definiens.com. Accessed 2012-10-23.

[70] Sousa AMO, Mesquita PA, Gonçalves AC, Marques da Silva JR. 2010. Segmentação e classificação de tipologias florestais a partir de imagens Quickbird. [Segmentation and classification of forest typologies using Quickbird images]. Ambiência (special edition). 2010;6:57–66.

[71] Esri. ArcGIS Desktop: Release 10. Redlands, CA: Environmental Systems Research Institute [Internet]. 2010. Available from: http://www.esri.com. Accessed 2013-01-23.

[72] Avery TE, Burkhart HE. editors. Forest Measurements. 4th ed. New York: McGraw-Hill Inc.; 1994. 480p.

[73] R Development Core Team. R: A Language and Environment for Statistical Computing. R Foundation for Statistical Computing [Internet]. 2012. Available from: http://www.R-project.org. Accessed 2013-02-21.

[74] Sheather SJ. editor. A Modern Approach to Regression with R. New York: Springer Texts in Statistics; 2009. 393 p.

[75] Legendre P, Legendre L. editors. Numerical Ecology. 3rd ed. Amsterdam: Elsevier Science BV. 2012; 24. 1006 p.

[76] Pretzsch H. editor. Forest Dynamics, Growth and Yield: From Measurement to Model. Berlin Heidelberg: Springer-Verlag; 2009. 664 p.

[77] Burkhart HE, Tomé M. Modelling Forest Trees and Stands. Dordrecht: Springer Science +Business Media; 2012. 457p.

[78] Clutter JL, Fortson JC, Pienaar LV, Briester GH, Bailey RL. editors. Timber Management: A Quantitative Approach. New York: John Wiley & Sons, Inc; 1983. 333p.

[79] Myers RH. editor. Classical and Modern Regression with Applications. Chicago: Duxbury Press; 1986. 488 p.

[80] Paulo JA, Palma JHN, Gomes AA, Faias SP, Tomé J, Tomé M. Predicting site index from climate and soil variables for cork oak (*Quercus suber* L.) stands in Portugal. New Forests. 2015;46:293–307.

[81] Congalton RG, Oderwald RG, Mead RA. Assessing Landsat classification accuracy using discrete multivariate statistical techniques. Photogrammetric Engineering and Remote Sensing. 1983;49:1671–1678.

[82] Stehman SV. Estimating the kappa coefficient and its variance under stratified random sampling. Photogrammetric Engineering & Remote Sensing. 1996;62:401–407.

[83] Oliver CD, Larson BC editors. Forest Stand Dynamics. Update editions. New York: John Wiley & Sons, Inc; 1996. 544p.

[84] Schütz JP. Sylviculture 2. La gestion des forêts irrégulières et mélangées. [Silviculture 2. The management of uneven aged and mixed forests]. Collection Gérer L'environement, no. 13. Lausanne: Presses Polytechniques et Universitaires Romandes; 1997. 178 p. [in French].

[85] Ke Y, Quackenbush LJ. A review of methods for automatic individual tree-crown detection and delineation from passive remote sensing. International Journal of Remote Sensing. 2011;32(17):4725–4747.

[86] Chemura A, Duren I, Leeuwen LM. Determination of the age of soil palm from crown projection area detected from WorldView-2 multispectral remote sensing data: the case of Ejisu-Juaben district, Ghana. ISPRS Journal of Photogrammetry and Remote Sensing. 2014;100:118–127.